Bioorthogonal correlative light-electron microscopy of mycobacterium tuberculosis in macrophages reveals the effect of antituberculosis drugs on subcellular bacterial distribution

Bakkum, T.; Heemskerk, M.T.; Bos, E.; Groenewold, M.; Oikonomeas-Koppasis, N.; Walburg, K.V.; ... ; Kasteren, S.I. van

Citation

ACS central science

Bioorthogonal Correlative Light-Electron Microscopy of *Mycobacterium tuberculosis* in Macrophages Reveals the Effect of Antituberculosis Drugs on Subcellular Bacterial Distribution

Thomas Bakkum, Matthias T. Heemskerk, Erik Bos, Mirjam Groenewold, Nikolaos Oikonomeas-Koppasis, Kimberley V. Walburg, Suzanne van Veen, Martijn J. C. van der Lienden, Tyrza van Leeuwen, Marielle C. Haks, Tom H. M. Ottenhoff, Abraham J. Koster, and Sander I. van Kasteren*

Read Online

ACCESS | Metrics & More | Article Recommendations | SI Supporting Information

ABSTRACT: Bioorthogonal correlative light-electron microscopy (B-CLEM) can give a detailed overview of multicomponent biological systems. It can provide information on the ultrastructural context of bioorthogonal handles and other fluorescent signals, as well as information about subcellular organization. We have here applied B-CLEM to the study of the intracellular pathogen *Mycobacterium tuberculosis* (*Mtb*) by generating a triply labeled *Mtb* through combined metabolic labeling of the cell wall and the proteome of a DsRed-expressing *Mtb* strain. Study of this pathogen in a B-CLEM setting was used to provide information about the intracellular distribution of the pathogen, as well as its *in situ* response to various clinical antibiotics, supported by flow cytometric analysis of the bacteria, after recovery from the host cell (*ex cellula*). The RNA polymerase-targeting drug rifampicin displayed the most prominent effect on subcellular distribution, suggesting the most direct effect on pathogenicity and/or viability, while the cell wall synthesis-targeting drugs isoniazid and ethambutol effectively rescued bacterial division-induced loss of metabolic labels. The three drugs combined did not give a more pronounced effect but rather an intermediate response, whereas gentamicin displayed a surprisingly strong additive effect on subcellular distribution.
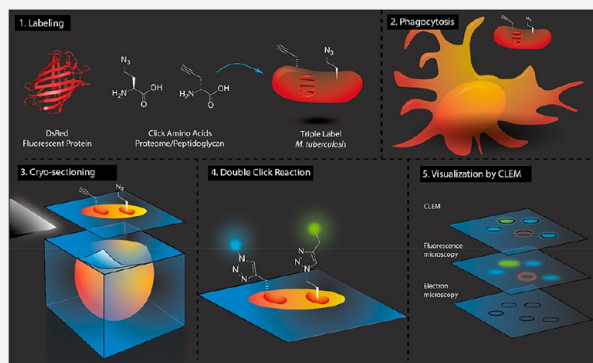
INTRODUCTION

Mycobacterium tuberculosis (*Mtb*), the causative agent of tuberculosis (TB), is currently the deadliest pathogen in the world. It is responsible for approximately 10 million cases and 1.6 million deaths every year.[1] Moreover, a quarter of the world's population is estimated to be carrying the latent form of the disease.[1] All this has become even more urgent over the last few decades with multidrug resistant (MDR-) and extensive drug resistant (XDR-) variants becoming increasingly prevalent.[1] Vaccine and drug development for *Mtb* has proven to be slow and challenging, in part due to the highly complex pathogen−host interactions and lack of suitable antigens.[2,3]

The intracellular lifecycle of *Mtb* further affects this problem. Upon infection of host cell macrophages, its behavior is highly heterogeneous: both fast- and slow-growing forms of the bacteria exist,[4,5] the latter displaying tolerance to most drugs.[6−12] This has resulted in the requirement for long treatment periods with cocktails of antibiotics, with the current standard of care being a six to nine-month course of rifampicin, isoniazid, ethambutol, and/or pyrazinamide.[13] Treatment of MDR-TB requires more extensive antibiotic treatment, lasting

up to 2 years, with poor side-effect profiles.[14] Recently, a new therapy for MDR-TB and XDR-TB was approved consisting of pretomanid in combination with bedaquiline and linezolid, and several others are currently under clinical development.[13]

Mtb is a facultative intracellular pathogen that primarily colonizes the lungs of patients by entering the upper and lower airways, through aerosol-transfer.[15] At these sites, *Mtb* is phagocytosed by alveolar macrophages, which—rather than clearing the pathogen—serve as their host cells.[16] The longstanding coevolution of *Mtb* with humans has resulted in the emergence of many mechanisms by which *Mtb* can interfere with the cellular and organismal immune responses.[17] It can, for example, inhibit phagosome acidification, block the recruitment of EEA1 and interfere with the Rab5-to-Rab7

conversion,[18] resulting in the formation of a nutrient rich compartment that favors survival and replication of the pathogen.[18,19] *Mtb* is also able to inhibit autophagy and apoptosis, effectively blocking all of the backup mechanisms for microbial killing.[20,21] Even if maturation of the phagosome does occur, *Mtb* is known to be strongly resistant to both acidic conditions (down to pH 4.5) and the reactive oxygen and nitrogen species (ROS/RNS) normally employed to kill phagosomal pathogens by virtue of its thick cell wall,[21] the production of antioxidative mycothiol (MSH),[21] and several neutralizing enzymes.[20,21]

It has recently been shown that the localization of *Mtb* within the cell is also a complex and highly dynamic process: some phagosomes are arrested in an early state, while the majority of phagosomes will follow the conventional maturation pathway, or a Rab20-dependent pathway to form a spacious phagosome.[22] Damaging of the phagosome allows the bacterium to avoid degradation or even escape to the cytosol, followed by rapid replication and host cell necrosis.[23] Recapture of the cytosolic bacteria may occur through ubiquitin-mediated autophagy, which again may lead to autophagosome maturation or arrest.[24−26] The precise contribution of these stages to overall *Mtb* survival is not yet known, nor is the change in this dynamic during drug treatment known; however, it implicates a dynamic host−pathogen "arms race". Even if a successful immune response—usually supported by T-cell help—is mounted against *Mtb*, generally a subpopulation of so-called "persister cells" remain in a dormant state. These bacteria have downregulated metabolic activity, upregulated stress-related genes, and as a result can establish a drug-tolerant, latent infection.[7]

This complex intracellular life cycle has made the study of *Mtb* difficult. Development of imaging techniques that allow the identification and study of the various stages of intracellular survival or killing of *Mtb* has been long sought after. Fluorescent protein-modified *Mtb* has allowed its imaging by confocal microscopy, but the reliability of fluorescent proteins varies and the fluorescence is lost upon degradation of the protein by the host.[27] Metabolic labeling of the mycobacterial cell wall, using fluorescent or bioorthogonal analogues of D-alanine[28,29] or trehalose,[30−32] or using fluorescent antibiotic analogues has allowed the study of growing and dividing *Mtb*.[33−35] This has, for example, allowed the discrimination of live from dead *Mtb* in sputum samples.[32] Finally, a dual-targeting activity-based probe was recently reported, combining the activity of two *Mtb*-specific enzymes to obtain extremely high specificity for *Mtb* over other mycobacteria.[36] These approaches are, however, all based on fluorescent techniques. This—in view of the complex life cycle of *Mtb* in the host—lacks information on, for example, host compartments and other ultrastructural features during infection.

Electron microscopy (EM) provides ultrastructural information but has limited options for labeling specific components of the bacterium and host, compared to fluorescent labeling techniques. For the study of *Mtb*, EM has proven useful to delineate parts of its life cycle, such as phagosome maturation, perturbation and repair, as well as cytosolic entry and reuptake by autophagy.[22,25,37−39] Correlative techniques, in which light and electron microscopy are combined, have proven to be powerful by providing both structural and functional information in one multimodal data set, that can be visualized in a single image. The combination of fluorescence microscopy and transmission electron microscopy (TEM) is known as correlative light-electron microscopy (CLEM).[40] For the study of *Mtb*, CLEM has been used to show *Mtb* replication within necrotic macrophages,[41] to discover a previously unknown niche for *Mtb* replication in the lymph nodes of TB patients,[42] and to visualize the subcellular distribution of bedaquiline in *Mtb*-infected macrophages.[43]

In order to combine the information that metabolic labeling studies can provide on the intracellular life cycle of *Mtb* with the information on bacterial structure and host cell biology that CLEM can provide, we decided to combine the two approaches. We have previously shown that the intracellular proteome labeled with alkyne or azide-containing amino acids can be selectively visualized by B-CLEM within a mammalian host cell (including degradation products stemming from the phagocytosed bacteria).[44,45] However, this only provided one parameter to study. We reasoned that, in order to provide a useful imaging approach for intracellular *Mtb*, multiple parameters relating to the intracellular lifecycle of the bacillus had to be visualized in parallel.

We here explore the option of combining two bioorthogonal labels in parallel—one for labeling the proteome and one for labeling the peptidoglycan layer—as well as the expression of a fluorescent protein. These three parameters, in combination with ultrastructural information, can yield information on where the bacteria are localized intracellularly, whether the bacteria are dividing, and to what extent antimycobacterials exert their antimicrobial effects. We describe a pathogen labeled with L-azidohomoalanine (Aha; proteome labeling), alkynyl-D-alanine (alkDala; peptidoglycan labeling), and DsRed (anabolic activity) and study its fate inside a macrophage cell line. Using dual copper-catalyzed Huisgen (ccHc) "click" labeling on thin sections, we could study these three parameters in their ultrastructural context. The two handles could be consecutively reacted without apparent cross-reactivity between handles (no loss of signal or altered patterns were observed compared to single labels). This B-CLEM approach allowed us to examine the intracellular distribution of the bacterium and link this information to the retention of the metabolic labels over time. Comparing these parameters between untreated cells and cells treated with rifampicin, isoniazid, ethambutol, or a combination of the three provided valuable insights into the subcellular effect of these clinical antibiotics. These observations were then further substantiated using a flow cytometry-based assay that allowed a more thorough quantification of the label retention under these conditions.

■ RESULTS AND DISCUSSION

Production and Validation of Triple-Label *Mtb*. We have previously optimized the incorporation of bioorthogonal amino acids in *E. coli* and *S. enterica* serovar Typhimurium, based on the BONCAT-protocol developed by the Tirrell-lab.[46−49] Using in-gel fluorescence after ccHc of bacterial lysates, label incorporation into the bacterial proteome could be quantified on the population level. Flow cytometry of fixed bacteria allowed the quantification of the label on a per-bacterium level.[44,45] These studies have yielded optimal labeling conditions consisting of a pulse with the bioorthogonal amino acid (4 mM) for approximately 1−2 doubling times (30 min in case of the above species). Whereas increased incubation led to reduced growth and viability.[44,45]

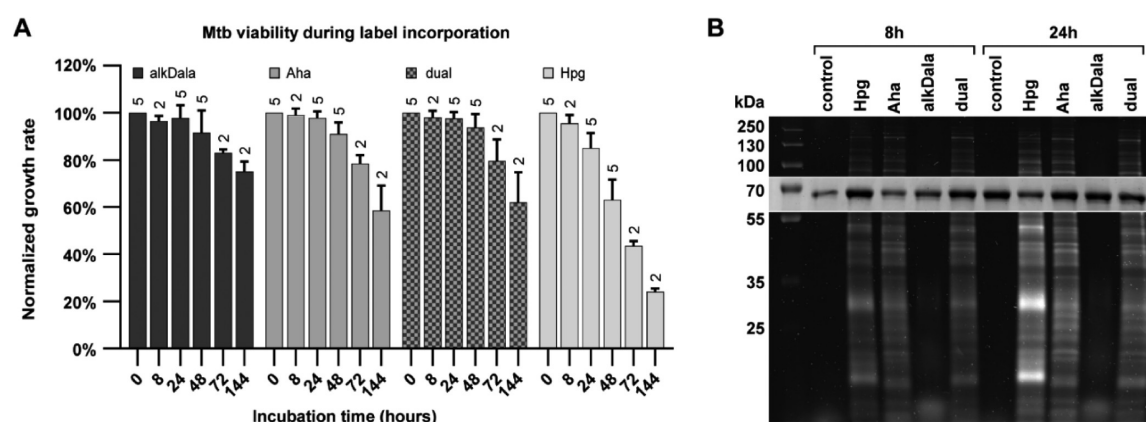In order to optimize bioorthogonal amino acid-incorporation into the *Mtb*-proteome, we first optimized the lysis

Figure 1. Production and validation of triple label Mtb. DsRed-expressing Mtb H37Rv were incubated with 4 mM Hpg, 4 mM Aha, 5 mM alkDala or a combination of 4 mM Aha and 5 mM alkDala (dual), for the indicated time in Middlebrook 7H9 broth. (A) Bacterial viability during label incorporation was assessed by normalizing the growth rate (OD_{600} measurements) to control bacteria, grown in the absence of metabolic labels. The number of biological replicates for each OD_{600} measurement is indicated above the bar; error bars indicate standard deviation from the mean. (B) Label incorporation throughout the proteome was analyzed by in-gel fluorescence, following bacterial lysis, ccHc reaction with AF647-azide (alkDala/Hpg) or AF647-alkyne (Aha/dual) and SDS-PAGE. Coomassie Brilliant Blue staining was used as a loading control; shown as an insert around the most prominent 60 kDa band, resulting from the DsRed-expression plasmid containing the Hsp60 promotor.[50]

conditions for *Mtb* to maximize protein recovery (and killing of the pathogen to allow handling outside the ML-III facility). This was achieved with a combination of 1% SDS and heat treatment, as we noticed that detergents alone were insufficient for both killing and protein recovery (Table S1). We used these lysis conditions to assess bioorthogonal amino acid incorporation. As the generation time of *Mtb* is approximately 24 h, we began exploring conditions starting from 4 mM azidohomoalanine (Aha) or homopropargylglycine (Hpg) for 48 h. We found that the label incorporation plateaued around 48 h but that labeling times >48 h reduced cell growth, particularly for homopropargylglycine-treated cells (Figure 1A). We therefore chose to focus on Aha for proteome labeling.

Cell wall labeling conditions with alkynyl-D-alanine (alkDala), a ccHc-reactive precursor in the cell wall synthesis, were taken from Siegrist et al., 2013.[28] Single labeling experiments with Aha or alkDala showed that no detrimental effects on viability were observed up to 48 h for either label in terms of viability (Figure 1A). Even extensively labeled *Mtb* (144 h) seemed to recover their growth rate after medium exchange (Figure S1). We next determined whether this was also the case for dual labeling with Aha and alkDala (Figure 1A, Figure S1). Coincubation of *Mtb* with both labels did not enhance toxicity up to the 48 h time point and revealed homogeneous proteome labeling (Figure 1B). From the gel-based incorporation assay, we concluded that treatment of *Mtb* for 48 h with both labels gave the optimal labeling (combined with the most facile protocol).

We next wanted to determine whether all cells incorporated the label to an equal extent in a flow cytometry-based assay. Again, previous protocols for bacterial fixation and permeabilization for flow cytometry were found to be incompatible with ccHc on *Mtb*. This was likely due to the thick (40−100 nm) and highly complex mycobacterial cell wall.[51] The mycobacterial cell wall contains multiple layers of (peptido)glycans and lipids, including the ultralipophilic mycolic acids that can be up to 90 carbons in length.[52] In practice, this results in hydrophobic aggregation of bacteria (especially after fixation) and an impermeability to the ccHc-reactive fluorophores. We postulated this would reduce the yields of the two ccHc-

reactions. We explored a wide range of permeabilization conditions, varying detergents, permeabilization, and fixation conditions (Table S2). After this extensive optimization, it was found that the most effective conditions for permeabilizing the bacteria for flow cytometric analysis—that balanced the permeability with the structural integrity required to remain intact during ccHc reaction—were pretreatment with 1% SDS for 15 min, followed by overnight fixation with 4% paraformaldehyde at room temperature (Table S2). Addition of BSA as an anticlumping additive during staining steps (Table S3) was needed to avoid hydrophobic aggregation of the fixed bacteria.

Despite this extensive set of optimization experiments, a subpopulation of DsRed positive events (~25%) remained unlabeled by both click reactions, perhaps due to them being dead before labeling, permeabilization resistant, or metabolically inactive.[7,53] They were excluded from quantification by gating for the double positive (Aha+/alkDala+) quadrant (Figure 2A, Figure S2). It was also shown that preincubation with Rifampicin for 1 and 24 h respectively reduced or abolished Aha-incorporation at 0.1, 1.0, and 10 µg/mL (Figure S3). The cell wall inhibitor D-cycloserine achieved the same for alkDala incorporation (Figure S4). Heat killing (Figure S5B) or paraformaldehyde fixation (Figure S5C) abolished the incorporation of both labels. With these restrictions applied, label incorporation for Aha and alkDala seemed to follow a similar trend as observed for the SDS-PAGE assay. Incorporation of both labels plateaued at 48 h incubation, with high signal-to-background (Figure 2A-viii).

Bioorthogonal CLEM as a Multiparameter Analysis Method to Study Intracellular *Mtb*. After successfully constructing triple label *Mtb*, their compatibility with our previously reported bioorthogonal CLEM method was assessed (Figure 2B, Figure 3). To this end, DsRed-expressing Mtb were incubated with Aha (4 mM) and alkDala (5 mM) simultaneously for 48 h for maximum label incorporation. The bacteria were prepared for cryo-sectioning, according to the Tokuyasu method.[54−56] Briefly, samples were fixed with paraformaldehyde and glutaraldehyde (2% w/v and 0.2% w/v respectively for 2 h), after which the bacterial pellet was rinsed with PBS and embedded in 12% gelatin. Millimeter-
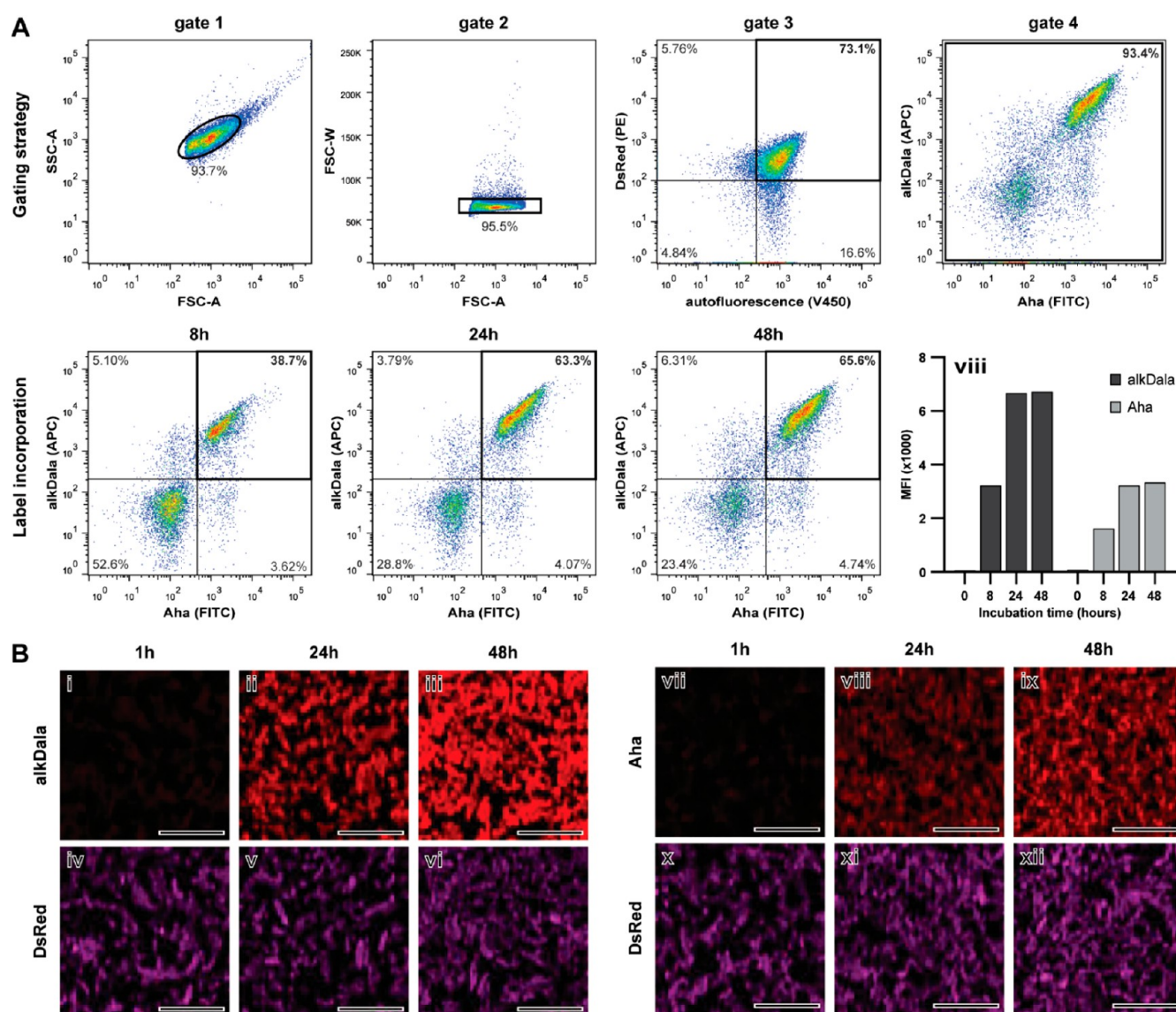
Figure 2. Optimization of label incorporation. DsRed-expressing *Mtb* H37Rv were incubated with 4 mM Aha, 5 mM alkDala or a combination of 4 mM Aha and 5 mM alkDala (dual), for the indicated time in Middlebrook 7H9 broth. (A) Label incorporation per bacterium was quantified by flow cytometry after sequential ccHc reaction with AF647-azide (alkDala) and AF488-alkyne (Aha) on fixed and permeabilized bacteria. Bacteria were selected based on size (gate 1), shape (gate 2), fluorescence (gate 3), and exclusion of extreme outliers (gate 4). Quantification of the label incorporation was achieved by selecting the median fluorescence intensity (MFI) of the major [Aha+/alkDala+] population for dually labeled *Mtb* or the major [Aha-/alkDala-] population for unlabeled *Mtb*. Controls and normalized MFI values are shown in Figure S2. (B) Triple label *Mtb* were processed for cryo-sectioning, followed by ccHc reaction with AF647-azide (alkDala) or AF647-alkyne (Aha), to confirm the increase in label incorporation over time on ultrathin sections that can be directly used for CLEM. All scale bars represent 5 μm.

sized cubes were prepared manually, followed by sucrose infiltration and plunge-freezing on sample pins. Ultrathin cryosections (75 nm) were prepared and transferred to a Formvar/carbon-coated titanium TEM-grid. Thawed cryo-sections were subjected to on section click-reaction with AF647-azide or AF647-alkyne for equal comparison between Aha and alkDala incorporation. Using these experiments, the label incorporations could be confirmed (with the sectioning being used in lieu of permeabilization). Both alkDala and Aha were minimally detectable after 1 h with the signal increasing upon longer incubation (Figure 2B). Optimal label incorporation is observed after 48 h without any noticeable effect on DsRed fluorescence. No detectable background fluorescence was observed for the unlabeled control samples (Figure S6).

Next, these single bacteria were imaged by B-CLEM: Fresh sections were prepared and subjected to double on-section click-reaction with AF647-azide and AF488-alkyne, with washing in between. The labeled sections were first imaged in the confocal microscope, then stained with uranyl acetate and imaged by TEM. The resulting images were then correlated using Photoshop to obtain the final CLEM images (Figure 3, Figure S7). These CLEM images show that >80% (*n* = 200) of bacteria were positive for alkDala, Aha and/or DsRed, suggesting suboptimal permeabilization was responsible for the incomplete labeling observed by flow cytometry above. The proteome label Aha colocalized largely with the fluorescent protein DsRed.

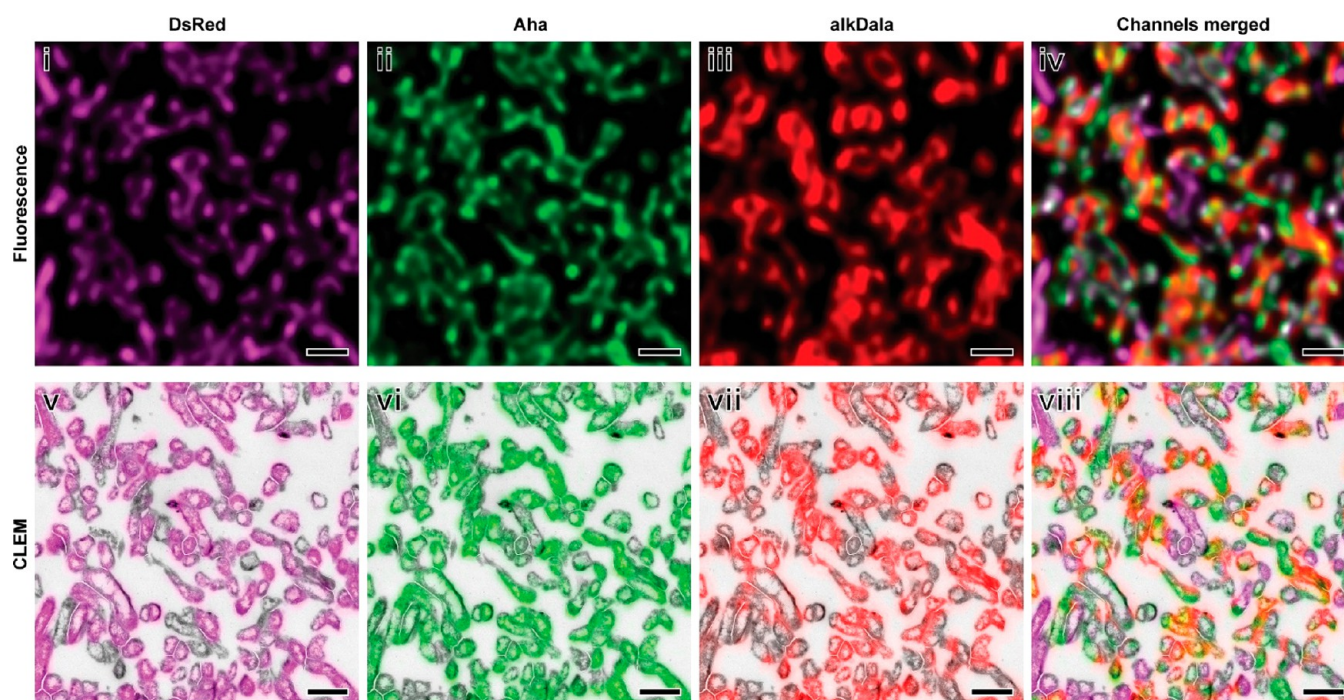To explore the possibility of studying intracellular Mtb localization and processing, we next infected a murine (LPS-

Figure 3. Bioorthogonal CLEM of triple label Mtb in vitro. Triple label Mtb were processed for cryo-sectioning, followed by sequential ccHc reaction with AF647-azide and AF488-alkyne. The fluorescently labeled sections were imaged by confocal microscopy, followed by TEM and the images were correlated to obtain the CLEM image. The lower panel shows details from the large field of view CLEM image presented in Figure S4. The top panel shows the corresponding fluorescence channels separately for clarity. All scale bars represent 1 μm.

stimulated) macrophage cell line (RAW 264.7)[57,58] with the double labeled DsRed-positive Mtb (MOI 25). We wanted to explore whether signs of viability could be extrapolated from the information-dense CLEM images, containing both the ultrastructural information on EM and the functional information on the multilabel fluorescence microscopy. After Tokuyasu sample preparation, we were able to obtain large field of view CLEM images containing over 100 cell-profiles per image at 11 000× magnification by applying an in-house developed EM-stitching algorithm.[59] This approach provides a large data set for qualitative and quantitative analysis of EM structures, guided by the fluorescence (illustrated in Figure S8). As observed in previous EM studies,[19,60] the mycobacterial cell wall shows a typical electron translucent layer, representing the mycomembrane (MM), enclosed by an electron-dense outer layer (OL) and the peptidoglycan layer (PGL) (Figure 4i). The bacterial cell wall is delineated by the signal distribution of alkDala (Figure 4iv). Mtb was found to be spread over different compartments, such as small or tight vacuoles (Figure 4v, Figure S9B), large or spacious vacuoles (Figure 4ix, Figure S9C), or what appeared to be non-membrane-bound compartments (which could be due an insufficient membrane preservation on EM) (Figure 4i, Figure S9A). The presence of Mtb in these apparently nonmembrane-bound compartments suggests escape from the parasitic vacuole to the cytosol, as been reported in multiple studies.[19,23,61−64] In some cases, a double membrane was observed in proximity of an apparently cytosolic bacterium (Figures S8D and S9A-iv), which is a hallmark of autophagy,[65] implying that this process may occur.

At 24 h postinfection, 23% of bacteria were found in small vacuoles, 72% in large vacuoles, and 5% with no detectable membrane (n > 500 bacteria counted). Additionally, a small percentage of bacteria (<5% of total) was found extracellularly,

surrounded by cell debris (illustrated in Figure S10A,B). Many large vacuoles contained both bacteria and cell debris, suggesting the bacteria could have escaped from the previous host cell,[23,66] before reuptake by another macrophage (Figure S10B). If host cell necrosis occurs, the plasma membrane integrity is lost, causing the cell to fall apart, which allows the bacteria to escape. However, if the host cell initiates apoptosis, the entire cell including bacteria can be taken up by a neighboring macrophage in a process called efferocytosis.[67] Distributions of bacteria indicative for either secondary phagocytosis of Mtb, following necrosis of the host cell (Figure S10C-i) or efferocytosis, when the entire apoptotic cell is internalized (Figure S10C-ii), were observed.

Bioorthogonal CLEM of Mtb-infected macrophages reveals the effect of antibiotics on the bacterial integrity and intracellular processing. To determine how the intracellular distribution and fluorescent signals of triple label Mtb would be affected by the commonly used antibiotics used in the treatment of tuberculosis, we repeated the experiment in the presence of rifampicin, isoniazid, ethambutol, or a combination of the three for 24 h. All drugs except ethambutol alone induced a significant alteration in the intracellular distribution of the bacteria (Figure 5A), with the triple-antibiotic cocktail showing the most pronounced effect, with 15% of bacteria residing in small vacuoles, 84% in large vacuoles, and only 1% did not appear to be within a vacuole (n > 500). Interestingly, when cells were incubated with heat-killed bacteria, 95% of all bacteria were found in large vacuoles, with <0.5% present in structures without a detectable membrane. The individual drugs had less pronounced effects on distribution (Figure 5A). Rifampicin caused the largest shift in subcellular localization, with 12% of bacteria residing in small vacuoles, 85% in large vacuoles, and 3% not within a vacuole (n > 500). Isoniazid had a less pronounced effect, with 20% of bacteria in small
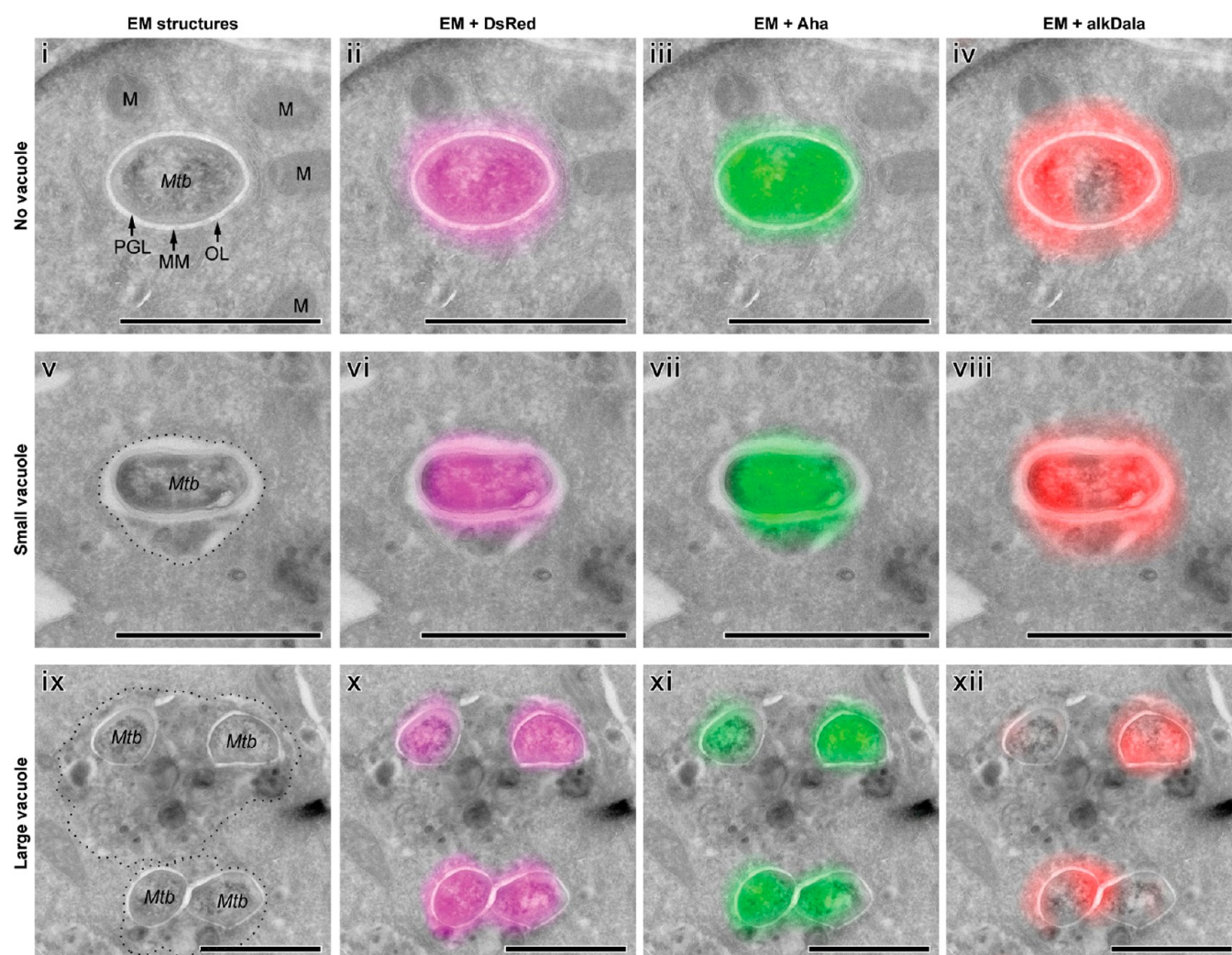
Figure 4. Bioorthogonal CLEM of triple label *Mtb* in RAW 264.7 macrophages. Triple label *Mtb* were processed for cryo-sectioning, followed by sequential ccHc reaction with AF647-azide and AF488-alkyne, and counterstaining with DAPI. Fluorescently labeled sections were imaged by confocal microscopy, followed by TEM and the images were correlated to obtain the CLEM image. The fuzziness of the fluorescent signal is a result of the difference in resolution between the techniques as governed by the Abbe-limit of diffraction. Representative examples of intracellular triple label *Mtb* are shown, not within a vacuole (i–iv), in a small/tight vacuole (v–viii), or in a large/spacious vacuole (ix–xii). Small field of view CLEM images with separated fluorescence channels are shown for clarity. Corresponding large field of view image is presented in Figure S5. N = nucleus, M = mitochondria, PGL = peptidoglycan layer, MM = mycomembrane, OL = outer layer. A dotted line indicates the apparent vacuole where relevant. All scale bars represent 1 μm.

vacuoles, 78% in large vacuoles, and 3% not within a vacuole ($n > 500$). Ethambutol did not show a significant difference compared to the control.

A large percentage of bacteria were found to be extracellular upon treatment with isoniazid (41% of total, $n > 500$) or ethambutol (12% of total, $n > 500$; Figure S11A), suggesting different drug mechanisms of action are involved. In addition, isoniazid treatment appeared to increase the occurrence of apparent host cell death (37%, $n > 500$), while ethambutol appeared to decrease host cell death (2%, $n > 500$; Figure S11B). These findings prompted us to reconsider our standard infection protocol, in which the infected cells are coincubated with a low concentration of gentamicin (5 μg/mL) to kill off extracellular bacteria. We hypothesized that during the 24 h of incubation, many bacteria could escape from the host cell and be affected by the extracellular gentamicin, before being taken up by another macrophage. This may result in an artificially high number of dead bacteria, leading to skewing in the relative

intracellular subpopulations. To test this, Mtb-infected cells were incubated with or without the triple-antibiotic cocktail, in the presence or absence of gentamicin, for 24 h and processed for CLEM. Indeed, a significant effect on the intracellular distribution was observed for both the triple-antibiotic cocktail and the untreated cells, when comparing the presence or absence of gentamicin (Figure 5B). Interestingly, a similar effect can be observed when comparing the triple-antibiotic cocktail to the control, either with gentamycin or without. This implies an additive drug effect for gentamicin, on top of the other antibiotics. Indeed, Mtb-infected cells in the complete absence of antibiotics showed only 50% of the bacteria residing in large vacuoles versus 31% in small vacuoles and 19% without an apparent vacuole ($n > 500$). Gentamicin was therefore excluded from all further experiments.

In addition to the intracellular distribution of Mtb, the shape of the bacterial profile appeared to be affected by the antibiotics as well. After (cryo-)sectioning of the rod-shaped
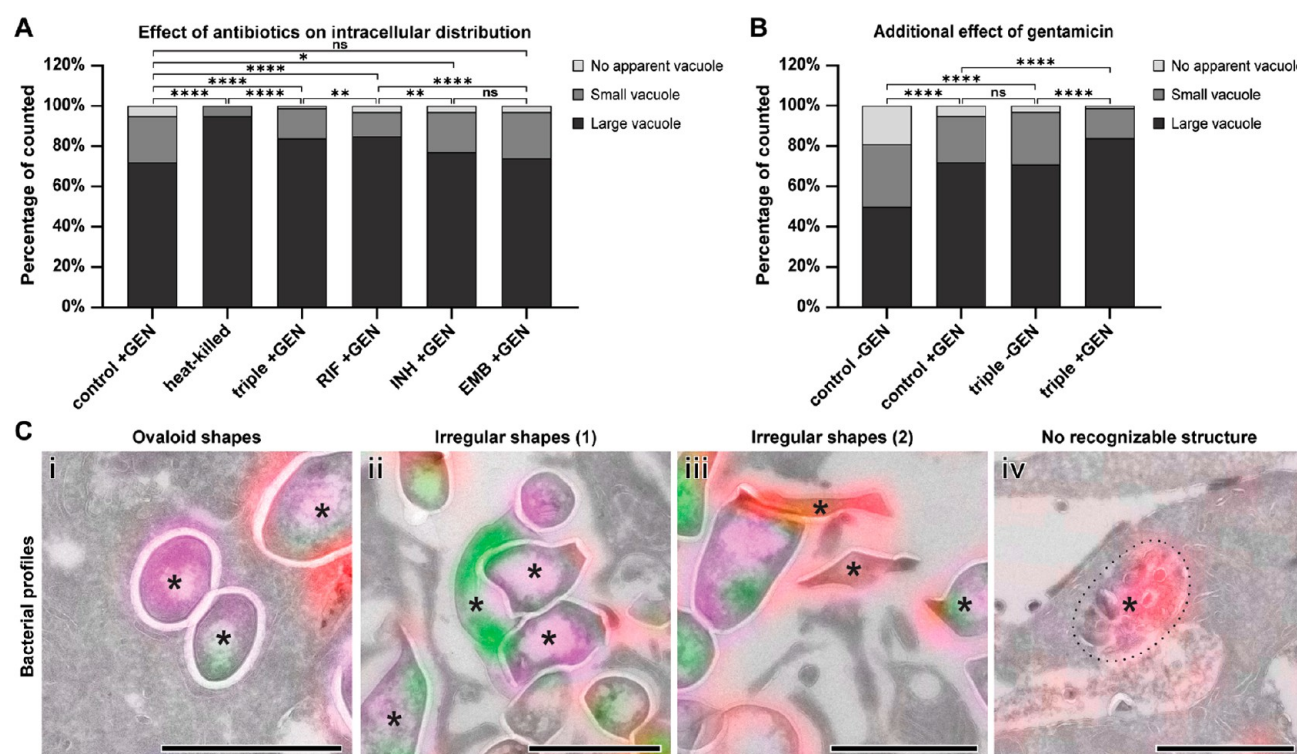
Figure 5. Effect of different antibiotics on the intracellular distribution and shape of triple label *Mtb* in RAW 264.7 macrophages. (A) Intracellular distribution of *Mtb* was manually classified as not within a vacuole (none), small/tight vacuole (small) or large/spacious vacuole (large), after 24 h of incubation with rifampicin (RIF), isoniazid (INH), ethambutol (EMB), triple antibiotics cocktail (triple), or without antibiotics (control). Shown as percentage relative to total number of intracellular *Mtb* counted in the analyzed region; $n > 500$ for all. (B) The additional effect of gentamicin (GEN) on the intracellular distribution of *Mtb* was assessed after 24 h of incubation with triple antibiotic cocktail (triple $\pm$GEN) or without antibiotics (control $\pm$GEN). Raw distributions were pairwise compared using the chi-square test and corrected for multiple testing using the Benjamini−Hochberg procedure, with a false discovery rate (FDR) of 0.1 (****: $p < 0.0001$, **: $p < 0.01$, *: $p < 0.05$, ns: not significant). (C) Zoom-in CLEM examples of the most common shapes, observed for bacterial profiles, classified as ovaloid (i), irregular (ii/iii), or no recognizable structure (iv; enhanced contrast of fluorescence for visual purposes). Relevant structures are indicated with an asterisk (*). A dotted line indicates the apparent vacuole where relevant. All scale bars represent 1 μm.
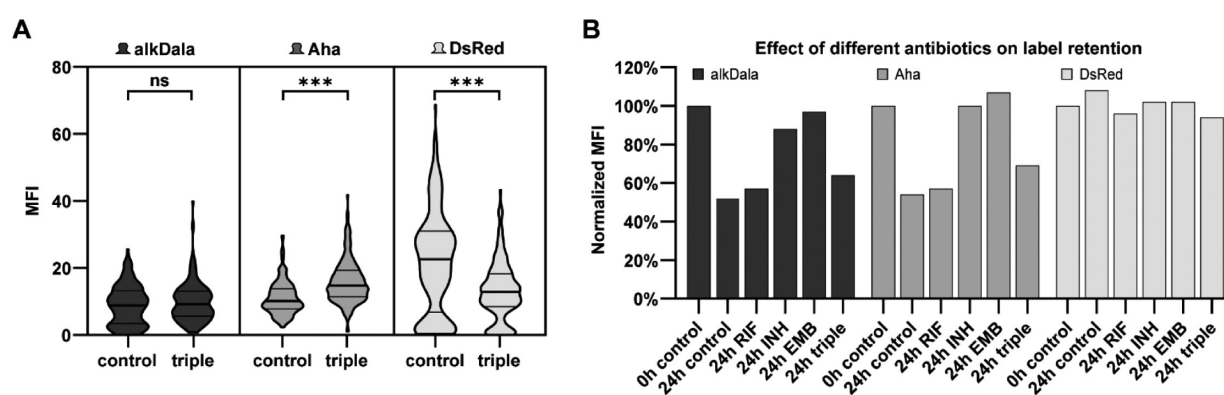

Figure 6. Quantification of label retention after intracellular incubation of triple label *Mtb* in RAW 264.7 macrophages with antibiotics. (A) CLEM-based semiautomatic quantification of label retention after 24 h intracellular incubation with triple antibiotics cocktail (triple) or without antibiotics (control). Distribution of the mean fluorescence intensity per bacterial profile ($n = 200$). Thick horizontal line represents population mean, thin horizontal lines represent standard deviation (***: $p < 0.001$, ns: not significant, Mann−Whitney U test). (B) Flow cytometry-based quantification of label retention *ex cellula*, after 24 h intracellular incubation with rifampicin (RIF), isoniazid (INH), ethambutol (EMB), triple antibiotic treatment (triple) or without antibiotics (24h control), normalized on bacteria recovered immediately after infection (0 h control). Corresponding dot plots and MFI values, before normalization, are shown in Figure S12.

Mtb, the expected bacterial profile is somewhere between circular and elongated, but always ovaloid in shape (Figure 5C-i). Indeed the bacterial profiles after 24 h of intracellular incubation without antibiotics were primarily ovaloid in shape (69%, $n > 500$; Figure S13D). The remaining bacterial profiles

display an irregular "pointy" shape (Figure 5C-ii/iii/S13B), perhaps suggesting a loss of bacterial integrity prior to fixation. Triple antibiotics treatment appeared to increase the number of irregular profiles (57%, $n > 500$; Figure S13D), which may indicate an increase in Mtb killing. Some vacuoles were even

found to contain distinct fluorescence while entirely lacking any recognizable bacterial structure (Figure 5C-iv, Figure S13C), potentially carrying degradation products of the labeled Mtb. Interestingly, heat-killed bacteria were predominantly observed as irregular shapes (95%, *n* > 500; Figure S13D) but with a well-preserved cell wall.

The early intracellular population of Mtb, immediately after infection, was highly concentrated in large vacuoles (>80%, *n* > 200). At this time point (0h postinfection), no significant effect of antibiotic pretreatment (24 h triple-antibiotic cocktail in vitro, before infection) on the subcellular distribution (Figure S12A) nor on the bacterial profiles of Mtb (Figure S13F) was observed, suggesting that more time is required for processing of the bacteria by the host cell. The untreated bacteria do appear to reside more in large clusters of smaller vacuoles, while the pretreated bacteria were mostly found in large and spacious vacuoles (see Figure S12B for examples). However, this classification criterium was too subtle for unbiased manual quantification.

CLEM and Flow Cytometry-Based Quantification of Mtb Label Retention upon Antibiotic Treatment. The average fluorescence intensity, resulting from the metabolic labels Aha and alkDala, can be used as a measure for bacterial division, as the label content per bacterium will "dilute" upon division. We were able to quantify the average fluorescence intensity per bacterium-profile from the images. First the bacteria were segmented, and the mean fluorescence intensity (MFI) was analyzed for each of the three fluorescence channels (*n* > 200 bacteria analyzed). DsRed-negative bacteria were excluded from analysis. These results show that intracellular Mtb, treated with the triple-antibiotic cocktail, retain more Aha and lose DsRed compared to the untreated control (Figure 6A, Figure S14). No significant difference in alkDala retention was observed (Figure 6B), although analysis artifacts due to the spreading of alkDala fluorescence beyond the selected bacterial outline (Figure S14), as well as variations in section thickness, cannot be excluded.

Since quantification of CLEM is intrinsically limited by its laborious correlation procedure, we set out to develop an additional method for quantifying the effect of antibiotics on bacterial proliferation that could support the observations done in CLEM. We therefore set up a method to analyze the bacteria by flow cytometry after recovery from the infected host cells (*ex cellula*). This was achieved by selective host cell lysis (adapted from Liu et al. 2015),[68] followed by fixation and click labeling of the recovered bacteria, using the method described above, to obtain optimal signal-to-noise and optimal recovery of bacteria.

The cytometry results show a clear loss of Aha and alkDala retention per bacterium over time (24 h vs 0 h control), in the absence of antibiotics (Figure 6B, Figure S15). This loss was largely avoided by isoniazid and ethambutol. Heat-killed bacteria showed no loss of label over time (Figure S16J). Rifampicin does not show an effect on label retention, suggesting a different mechanism of action (Figure 6B, Figure S15, Figure S16). The triple-antibiotic cocktail showed an intermediate effect on label retention, suggesting a combinatorial but nonadditive effect on label retention. No significant effect on DsRed was observed for any of the antibiotics, through this quantification approach. However, isoniazid and ethambutol show a distinct reduction in the typical Mtb autofluorescence,[69] similar but to a smaller degree as heat-killed Mtb (Figure S16F). This reduction in autofluorescence

has previously been suggested as an indication for mycobacterial viability.[70]

Taken together, our results indicate that—within the context of our LPS-stimulated murine macrophage infection system—rifampicin mostly affects Mtb pathogenicity, while isoniazid and ethambutol seem to affect Mtb division more directly; although the complexity and heterogeneity of the life cycle of Mtb in host cells remains profound.

◼ CONCLUSIONS

We describe a combinatorial method for studying the intracellular localization of pathogenic bacteria *in situ* and the effect of clinical or experimental drugs on the entire host—pathogen system. By combining fluorescent protein expression, proteome and cell wall labeling with high-content CLEM and flow cytometry, we were able to obtain new information about the complex intracellular behavior of *Mtb* in macrophages. CLEM allows for simple fluorescence-guided detection of bacterial structures, and inversely, EM-guided analysis of fluorescent labels. The ultrastructural information on EM provides a subcellular description of both the bacterial behavior and that of the host cell. In addition, flow cytometry provides a quantification method for bacterial label retention under varying conditions. Using a triple labeling strategy, different components of the bacterium could be visualized, providing multiparameter information about the metabolic state of the pathogen, although the sought-after *in vivo* unambigious identification of live, dormant, and dead bacteria remains beyond our grasp. Using multiple labels also significantly reduces the chance of missing events due to absence of a fluorescent label and, at the minimum, provides an internal standard for equivalent labels (Aha and alkDala). Alternatively, using a single bioorthogonal label could bypass the arduous task of genetically labeling a complicated level-3 pathogen, like *Mtb*.

We observed large differences between intracellular distribution of *Mtb* under normal conditions versus treatment with various clinical antibiotics. Rifampicin displayed the clearest effect on distribution, while isoniazid and ethambutol only had a mild effect. These observations suggest a more direct effect of rifampicin on bacterial pathogenicity and/or viability, which is in agreement with its proposed mechanism of action.[71] Surprisingly, a routine low dose of gentamicin displayed a strong effect on distribution, which was additive to both untreated cells or cells treated with all three antibiotics simultaneously. We hypothesized that this was due to bacteria escaping from the host cell, undergoing gentamicin-induced extracellular killing, followed by reinternalization by surrounding macrophages. Although this effect is unlikely to interfere with routine readouts, due to its additive nature, we caution others to consider a potential bias on drug efficacy. Flow cytometry-based quantification of label retention showed a clear loss of label retention over time, which was almost completely rescued by isoniazid or ethambutol treatment but to a far lesser extent by rifampicin or the triple antibiotics combination. Label dilution over time is expected due to bacterial division with no additional metabolic labels present in the medium. Label retention over time is therefore a result of inhibition of bacterial division, which is in accordance with the proposed mechanism of action for these antibiotics.[71] Perhaps most surprising is the apparently intermediate efficacy of the triple antibiotic combination, both in terms of bacterial distribution and label retention.

Besides broadly occurring phenomena, such as the subcellular distribution of *Mtb*, we observed many less common events such as apparent phagosome-lysosome fusion, possible autophagy of cytosolic *Mtb*, partially degraded *Mtb* fragments, leakage, and vesicular transport of fluorescently labeled *Mtb* components, bacterial lipid inclusions and exocytosis of mycolic acids. Although these observations could not yet be supported by sufficient evidence, they present an interesting starting point for follow-up studies, highlighting the exploratory power of CLEM.

■ EXPERIMENTAL INFORMATION

Details of all experiments can be found in the Supporting Information.

■ ASSOCIATED CONTENT

Ⓢ Supporting Information

The Supporting Information is available free of charge at https://pubs.acs.org/doi/10.1021/acscentsci.0c00539.

Full experimental details (PDF)

■ AUTHOR INFORMATION

Corresponding Author

Sander I. van Kasteren − *Leiden Institute of Chemistry and The Institute of Chemical Immunology, Leiden University, Leiden 2300 RA, The Netherlands;* ⓞ orcid.org/0000-0003-3733-818X; Email: s.i.van.kasteren@chem.leidenuniv.nl

Authors

Thomas Bakkum − *Leiden Institute of Chemistry and The Institute of Chemical Immunology, Leiden University, Leiden 2300 RA, The Netherlands*

Matthias T. Heemskerk − *Department of Infectious Diseases, Leiden University Medical Center, 2333 ZC Leiden, The Netherlands*

Erik Bos − *Department of Cell and Chemical Biology, Leiden University Medical Center, 2333 ZC Leiden, The Netherlands*

Mirjam Groenewold − *Leiden Institute of Chemistry and The Institute of Chemical Immunology, Leiden University, Leiden 2300 RA, The Netherlands*

Nikolaos Oikonomeas-Koppasis − *Leiden Institute of Chemistry and The Institute of Chemical Immunology, Leiden University, Leiden 2300 RA, The Netherlands*

Kimberley V. Walburg − *Department of Infectious Diseases, Leiden University Medical Center, 2333 ZC Leiden, The Netherlands*

Suzanne van Veen − *Department of Infectious Diseases, Leiden University Medical Center, 2333 ZC Leiden, The Netherlands*

Martijn J. C. van der Lienden − *Leiden Institute of Chemistry and The Institute of Chemical Immunology, Leiden University, Leiden 2300 RA, The Netherlands*

Tyrza van Leeuwen − *Leiden Institute of Chemistry and The Institute of Chemical Immunology, Leiden University, Leiden 2300 RA, The Netherlands*

Marielle C. Haks − *Department of Infectious Diseases, Leiden University Medical Center, 2333 ZC Leiden, The Netherlands*

Tom H. M. Ottenhoff − *Department of Infectious Diseases, Leiden University Medical Center, 2333 ZC Leiden, The Netherlands*

Abraham J. Koster − *Department of Cell and Chemical Biology, Leiden University Medical Center, 2333 ZC Leiden, The Netherlands*

Complete contact information is available at:
https://pubs.acs.org/10.1021/acscentsci.0c00539

■ REFERENCES

(1) World Health Organization (WHO). *Global Tuberculosis Report 2018*; WHO: Geneva, Switzerland, 2018.

(2) Fletcher, H. A.; Voss, G.; Casimiro, D.; Neyrolles, O.; Williams, A.; Kaufmann, S. H. E.; McShane, H.; Hatherill, M. Progress and Challenges in TB Vaccine Development. *F1000Research* **2018**, *7* (Mvi), 199.

(3) Schluger, N. W. Host-Pathogen Interactions in Tuberculosis: The Evolving Story. *J. Infect. Dis.* **2016**, *214* (8), 1137−1138.

(4) Bald, D.; Villellas, C.; Lu, P.; Koul, A. Targeting Energy Metabolism in Mycobacterium Tuberculosis, a New Paradigm in Antimycobacterial Drug Discovery. *mBio* **2017**, *8* (2), 1−11.

(5) Jnawali, H. N.; Ryoo, S. First - and Second - Line Drugs and Drug Resistance. In *Tuberculosis - Current Issues in Diagnosis and Management*; Mahboub, B. H., Vats, M. G., Eds.; InTech, 2013; pp 163−180.

(6) Deb, C.; Lee, C. M.; Dubey, V. S.; Daniel, J.; Abomoelak, B.; Sirakova, T. D.; Pawar, S.; Rogers, L.; Kolattukudy, P. E. A Novel in Vitro Multiple-Stress Dormancy Model for Mycobacterium Tuberculosis Generates a Lipid-Loaded, Drug-Tolerant, Dormant Pathogen. *PLoS One* **2009**, *4* (6), e6077.

(7) Dutta, N. K.; Karakousis, P. C. Latent Tuberculosis Infection: Myths, Models, and Molecular Mechanisms. *Microbiol. Mol. Biol. Rev.* **2014**, *78* (3), 343−371.

(8) Baker, J. J.; Abramovitch, R. B. Genetic and Metabolic Regulation of Mycobacterium Tuberculosis Acid Growth Arrest. *Sci. Rep.* **2018**, *8* (1), 4168.

(9) Daniel, J.; Maamar, H.; Deb, C.; Sirakova, T. D.; Kolattukudy, P. E. Mycobacterium Tuberculosis Uses Host Triacylglycerol to Accumulate Lipid Droplets and Acquires a Dormancy-like Phenotype in Lipid-Loaded Macrophages. *PLoS Pathog.* **2011**, *7* (6), No. e1002093.

(10) Pullan, S. T.; Allnutt, J. C.; Devine, R.; Hatch, K. A.; Jeeves, R. E.; Hendon-Dunn, C. L.; Marsh, P. D.; Bacon, J. The Effect of Growth Rate on Pyrazinamide Activity in Mycobacterium Tuberculosis - Insights for Early Bactericidal Activity? *BMC Infect. Dis.* **2016**, *16* (1), 1−11.

(11) Evangelopoulos, D.; Fonseca, J. D. da; Waddell, S. J. Understanding Anti-Tuberculosis Drug Efficacy: Rethinking Bacterial Populations and How We Model Them. *Int. J. Infect. Dis.* **2015**, *32*, 76−80.

(12) Sarathy, J. P.; Via, L. E.; Weiner, D.; Blanc, L.; Boshoff, H.; Eugenin, E. A.; Barry, C. E.; Dartois, V. A. Extreme Drug Tolerance of Mycobacterium Tuberculosis in Caseum. *Antimicrob. Agents Chemother.* **2018**, *62* (2), 1−11.

(13) Hoagland, D. T.; Liu, J.; Lee, R. B.; Lee, R. E. New Agents for the Treatment of Drug-Resistant Mycobacterium Tuberculosis. *Adv. Drug Delivery Rev.* **2016**, *102*, 55−72.

(14) Sarkar, S.; Ganguly, A. Current Overview of Anti-Tuberculosis Drugs: Metabolism and Toxicities. *Mycobact. Dis.* **2016**, *6* (2), 1−6.

(15) Philips, J. a.; Ernst, J. D. Tuberculosis Pathogenesis and Immunity. *Annu. Rev. Pathol.: Mech. Dis.* **2012**, *7* (1), 353−384.

(16) North, R. J.; Jung, Y.-J. Immunity to Tuberculosis. *Annu. Rev. Immunol.* **2004**, *22* (1), 599−623.

(17) Wilburn, K. M.; Fieweger, R. A.; VanderVen, B. C. Cholesterol and Fatty Acids Grease the Wheels of Mycobacterium Tuberculosis Pathogenesis. *Pathog. Dis.* **2018**, *76* (2), 1−14.

(18) Omotade, T. O.; Roy, C. R. Manipulation of Host Cell Organelles by Intracellular Pathogens. In *Bacteria and Intracellularity*; Cossart, P., Roy, C., Sansonetti, P., Eds.; ASM Press: Washington, DC, 2019; pp 199−214.

(19) van der Wel, N.; Hava, D.; Houben, D.; Fluitsma, D.; van Zon, M.; Pierson, J.; Brenner, M.; Peters, P. J. M. Tuberculosis and M. Leprae Translocate from the Phagolysosome to the Cytosol in Myeloid Cells. *Cell* **2007**, *129* (7), 1287−1298.

(20) Zhai, W.; Wu, F.; Zhang, Y.; Fu, Y.; Liu, Z. The Immune Escape Mechanisms of Mycobacterium Tuberculosis. *Int. J. Mol. Sci.* **2019**, *20* (2), 340.

(21) Ehrt, S.; Schnappinger, D. Mycobacterial Survival Strategies in the Phagosome: Defense against Host Stresses. *Cell. Microbiol.* **2009**, *11* (8), 1170−1178.

(22) Schnettger, L.; Rodgers, A.; Repnik, U.; Lai, R. P.; Pei, G.; Verdoes, M.; Wilkinson, R. J.; Young, D. B.; Gutierrez, M. G. A Rab20-Dependent Membrane Trafficking Pathway Controls M. Tuberculosis Replication by Regulating Phagosome Spaciousness and Integrity. *Cell Host Microbe* **2017**, *21* (5), 619−628.

(23) Simeone, R.; Bobard, A.; Lippmann, J.; Bitter, W.; Majlessi, L.; Brosch, R.; Enninga, J. Phagosomal Rupture by Mycobacterium Tuberculosis Results in Toxicity and Host Cell Death. *PLoS Pathog.* **2012**, *8* (2), e1002507.

(24) Romagnoli, A.; Etna, M. P.; Giacomini, E.; Pardini, M.; Remoli, M. E.; Corazzari, M.; Falasca, L.; Goletti, D.; Gafa, V.; Simeone, R.; Delogu, G.; Piacentini, M.; Brosch, R.; Fimia, G. M.; Coccia, E. M. ESX-1 Dependent Impairment of Autophagic Flux by Mycobacterium Tuberculosis in Human Dendritic Cells. *Autophagy* **2012**, *8* (9), 1357−1370.

(25) Lerner, T. R.; de Souza Carvalho-Wodarz, C.; Repnik, U.; Russell, M. R. G.; Borel, S.; Diedrich, C. R.; Rohde, M.; Wainwright, H.; Collinson, L. M.; Wilkinson, R. J.; Griffiths, G.; Gutierrez, M. G. Lymphatic Endothelial Cells Are a Replicative Niche for Mycobacterium Tuberculosis. *J. Clin. Invest.* **2016**, *126* (3), 1093−1108.

(26) Kimmey, J. M.; Stallings, C. L. Bacterial Pathogens versus Autophagy: Implications for Therapeutic Interventions. *Trends Mol. Med.* **2016**, *22* (12), 1060−1076.

(27) MacGilvary, N. J.; Tan, S. Fluorescent Mycobacterium Tuberculosis Reporters: Illuminating Host-Pathogen Interactions. *Pathog. Dis.* **2018**, *76* (3), 1−12.

(28) Siegrist, M. S.; Whiteside, S.; Jewett, J. C.; Aditham, A.; Cava, F.; Bertozzi, C. R. D-Amino Acid Chemical Reporters Reveal Peptidoglycan Dynamics of an Intracellular Pathogen. *ACS Chem. Biol.* **2013**, *8* (3), 500−505.

(29) Botella, H.; Yang, G.; Ouerfelli, O.; Ehrt, S.; Nathan, C. F.; Vaubourgeix, J. Distinct Spatiotemporal Dynamics of Peptidoglycan Synthesis between Mycobacterium Smegmatis and Mycobacterium Tuberculosis. *mBio* **2017**, *8* (5), 12−14.

(30) Backus, K. M.; Boshoff, H. I.; Barry, C. E. C. S.; Boutureira, O.; Patel, M. K.; D'Hooge, F.; Lee, S. S.; Via, L. E.; Tahlan, K.; Barry, C. E. C. S.; Davis, B. G. Uptake of Unnatural Trehalose Analogs as a Reporter for Mycobacterium Tuberculosis. *Nat. Chem. Biol.* **2011**, *7* (4), 228−235.

(31) Hodges, H. L.; Brown, R. A.; Crooks, J. A.; Weibel, D. B.; Kiessling, L. L. Imaging Mycobacterial Growth and Division with a Fluorogenic Probe. *Proc. Natl. Acad. Sci. U. S. A.* **2018**, *115* (20), 5271−5276.

(32) Kamariza, M.; Shieh, P.; Ealand, C. S.; Peters, J. S.; Chu, B.; Rodriguez-Rivera, F. P.; Babu Sait, M. R.; Treuren, W. V.; Martinson, N.; Kalscheuer, R.; Kana, B. D.; Bertozzi, C. R. Rapid Detection of Mycobacterium Tuberculosis in Sputum with a Solvatochromic Trehalose Probe. *Sci. Transl. Med.* **2018**, *10* (430), No. eaam6310.

(33) Yang, D.; Ding, F.; Mitachi, K.; Kurosu, M.; Lee, R. E.; Kong, Y. A Fluorescent Probe for Detecting Mycobacterium Tuberculosis and Identifying Genes Critical for Cell Entry. *Front. Microbiol.* **2016**, *7* (DEC), 2021.

(34) Cheng, Y.; Xie, H.; Sule, P.; Hassounah, H.; Graviss, E. A.; Kong, Y.; Cirillo, J. D.; Rao, J. Fluorogenic Probes with Substitutions at the 2 and 7 Positions of Cephalosporin Are Highly BlaC-Specific

for Rapid Mycobacterium Tuberculosis Detection. *Angew. Chem., Int. Ed.* **2014**, *53* (35), 9360−9364.

(35) Stone, M. R. L.; Butler, M. S.; Phetsang, W.; Cooper, M. A.; Blaskovich, M. A. T. Fluorescent Antibiotics: New Research Tools to Fight Antibiotic Resistance. *Trends Biotechnol.* **2018**, *36* (5), 523−536.

(36) Cheng, Y.; Xie, J.; Lee, K.-H.; Gaur, R. L.; Song, A.; Dai, T.; Ren, H.; Wu, J.; Sun, Z.; Banaei, N.; Akin, D.; Rao, J. Rapid and Specific Labeling of Single Live *Mycobacterium Tuberculosis* with a Dual-Targeting Fluorogenic Probe. *Sci. Transl. Med.* **2018**, *10* (454), No. eaar4470.

(37) Armstrong, J. A.; Hart, P. D. Response of Cultured Macrophages to Mycobacterium Tuberculosis, with Observations on Fusion of Lysosomes with Phagosomes. *J. Exp. Med.* **1971**, *134* (3), 713−740.

(38) Leake, E. S.; Myrvik, Q. N.; Wright, M. J. Phagosomal Membranes of Mycobacterium Bovis BCG-Immune Alveolar Macrophages Are Resistant to Disruption by Mycobacterium Tuberculosis H37Rv. *Infect. Immun.* **1984**, *45* (2), 443−446.

(39) McDonough, K. A.; Kress, Y.; Bloom, B. R. The Interaction of Mycobacterium Tuberculosis with Macrophages: A Study of Phagolysosome Fusion. *Infect. Agents Dis.* **1993**, *2* (4), 232−235.

(40) de Boer, P.; Hoogenboom, J. P.; Giepmans, B. N. G. Correlated Light and Electron Microscopy: Ultrastructure Lights Up! *Nat. Methods* **2015**, *12* (6), 503−513.

(41) Lerner, T. R.; Borel, S.; Greenwood, D. J.; Repnik, U.; Russell, M. R. G.; Herbst, S.; Jones, M. L.; Collinson, L. M.; Griffiths, G.; Gutierrez, M. G. Mycobacterium Tuberculosis Replicates within Necrotic Human Macrophages. *J. Cell Biol.* **2017**, *216* (3), 583−594.

(42) Russell, M. R. G.; Lerner, T. R.; Burden, J. J.; Nkwe, D. O.; Pelchen-Matthews, A.; Domart, M. C.; Durgan, J.; Weston, A.; Jones, M. L.; Peddie, C. J.; Carzaniga, R.; Florey, O.; Marsh, M.; Gutierrez, M. G.; Collinson, L. M. 3D Correlative Light and Electron Microscopy of Cultured Cells Using Serial Blockface Scanning Electron Microscopy. *J. Cell Sci.* **2017**, *130* (1), 278−291.

(43) Greenwood, D. J.; Dos Santos, M. S.; Huang, S.; Russell, M. R. G.; Collinson, L. M.; MacRae, J. I.; West, A.; Jiang, H.; Gutierrez, M. G. Subcellular Antibiotic Visualization Reveals a Dynamic Drug Reservoir in Infected Macrophages. *Science* **2019**, *364* (6447), 1279−1282.

(44) van Elsland, D. M.; Bos, E.; de Boer, W.; Overkleeft, H. S.; Koster, A. J.; van Kasteren, S. I. Detection of Bioorthogonal Groups by Correlative Light and Electron Microscopy Allows Imaging of Degraded Bacteria in Phagocytes. *Chem. Sci.* **2016**, *7* (1), 752−758.

(45) van Elsland, D. M.; Pujals, S.; Bakkum, T.; Bos, E.; Oikonomeas-Koppasis, N.; Berlin, I.; Neefjes, J.; Meijer, A. H.; Koster, A. J.; Albertazzi, L.; van Kasteren, S. I. Ultrastructural Imaging of Salmonella-Host Interactions Using Super-Resolution Correlative Light-Electron Microscopy of Bioorthogonal Pathogens. *ChemBioChem* **2018**, *19* (16), 1766−1770.

(46) Van Hest, J. C. M.; Kiick, K. L.; Tirrell, D. A. Efficient Incorporation of Unsaturated Methionine Analogues into Proteins in Vivo. *J. Am. Chem. Soc.* **2000**, *122* (7), 1282−1288.

(47) Kiick, K. L.; Saxon, E.; Tirrell, D. a; Bertozzi, C. R. Incorporation of Azides into Recombinant Proteins for Chemoselective Modification by the Staudinger Ligation. *Proc. Natl. Acad. Sci. U. S. A.* **2002**, *99* (1), 19−24.

(48) Dieterich, D. C.; Link, A. J.; Graumann, J.; Tirrell, D. A.; Schuman, E. M. Selective Identification of Newly Synthesized Proteins in Mammalian Cells Using Bioorthogonal Noncanonical Amino Acid Tagging (BONCAT). *Proc. Natl. Acad. Sci. U. S. A.* **2006**, *103* (25), 9482−9487.

(49) Hatzenpichler, R.; Scheller, S.; Tavormina, P. L.; Babin, B. M.; Tirrell, D. A.; Orphan, V. J. In Situ Visualization of Newly Synthesized Proteins in Environmental Microbes Using Amino Acid Tagging and Click Chemistry. *Environ. Microbiol.* **2014**, *16* (8), 2568−2590.

(50) Korbee, C. J.; Heemskerk, M. T.; Kocev, D.; Van Strijen, E.; Rabiee, O.; Franken, K. L. M. C.; Wilson, L.; Savage, N. D. L.; Džeroski, S.; Haks, M. C.; Ottenhoff, T. H. M. Combined Chemical

Genetics and Data-Driven Bioinformatics Approach Identifies Receptor Tyrosine Kinase Inhibitors as Host-Directed Antimicrobials. *Nat. Commun.* **2018**, *9* (1), 358.

(51) Vincent, A. T.; Nyongesa, S.; Morneau, I.; Reed, M. B.; Tocheva, E. I.; Veyrier, F. J. The Mycobacterial Cell Envelope: A Relict from the Past or the Result of Recent Evolution? *Front. Microbiol.* **2018**, *9* (OCT), 1–9.

(52) Daffé, M.; Quémard, A.; Marrakchi, H. Mycolic Acids: From Chemistry to Biology. In *Biogenesis of Fatty Acids, Lipids and Membranes*; Geiger, O., Ed.; Springer: Cham, 2017; pp 1–36.

(53) Gengenbacher, M.; Kaufmann, S. H. E. Mycobacterium Tuberculosis: Success through Dormancy. *FEMS Microbiol. Rev.* **2012**, *36* (3), 514–532.

(54) Tokuyasu, K. T. A Technique for Ultracryotomy of Cell Suspensions and Tissues. *J. Cell Biol.* **1973**, *57* (2), 551–565.

(55) Peters, P. J.; Bos, E.; Griekspoor, A. Cryo-Immunogold Electron Microscopy. *Curr. Protoc. Cell Biol.* **2006**, *30* (1), 4.7.1–4.7.19.

(56) Möbius, W.; Posthuma, G. Sugar and Ice: Immunoelectron Microscopy Using Cryosections According to the Tokuyasu Method. *Tissue Cell* **2019**, *57* (July), 90–102.

(57) Gupta, A.; Bhakta, S. An Integrated Surrogate Model for Screening of Drugs against Mycobacterium Tuberculosis. *J. Antimicrob. Chemother.* **2012**, *67* (6), 1380–1391.

(58) Wang, X.; Grace, P. M.; Pham, M. N.; Cheng, K.; Strand, K. A.; Smith, C.; Li, J.; Watkins, L. R.; Yin, H. Rifampin Inhibits Toll-like Receptor 4 Signaling by Targeting Myeloid Differentiation Protein 2 and Attenuates Neuropathic Pain. *FASEB J.* **2013**, *27* (7), 2713–2722.

(59) Faas, F. G. A.; Cristina Avramut, M.; van den Berg, B. M.; Mieke Mommaas, A.; Koster, A. J.; Ravelli, R. B. G. Virtual Nanoscopy: Generation of Ultra-Large High Resolution Electron Microscopy Maps. *J. Cell Biol.* **2012**, *198* (3), 457–469.

(60) Vijay, S.; Hai, H. T.; Thu, D. D. A.; Johnson, E.; Pielach, A.; Phu, N. H.; Thwaites, G. E.; Thuong, N. T. T. Ultrastructural Analysis of Cell Envelope and Accumulation of Lipid Inclusions in Clinical Mycobacterium Tuberculosis Isolates from Sputum, Oxidative Stress, and Iron Deficiency. *Front. Microbiol.* **2018**, *8* (JAN), 1–12.

(61) Acosta, Y.; Zhang, Q.; Rahaman, A.; Ouellet, H.; Xiao, C.; Sun, J.; Li, C. Imaging Cytosolic Translocation of Mycobacteria with Two-Photon Fluorescence Resonance Energy Transfer Microscopy. *Biomed. Opt. Express* **2014**, *5* (11), 3990.

(62) Houben, D.; Demangel, C.; van Ingen, J.; Perez, J.; Baldeón, L.; Abdallah, A. M.; Caleechurn, L.; Bottai, D.; van Zon, M.; de Punder, K.; van der Laan, T.; Kant, A.; Bossers-De Vries, R.; Willemsen, P.; Bitter, W.; van Soolingen, D.; Brosch, R.; van der Wel, N.; Peters, P. J. ESX-1-Mediated Translocation to the Cytosol Controls Virulence of Mycobacteria. *Cell. Microbiol.* **2012**, *14* (8), 1287–1298.

(63) Simeone, R.; Sayes, F.; Song, O.; Gröschel, M. I.; Brodin, P.; Brosch, R.; Majlessi, L. Cytosolic Access of Mycobacterium Tuberculosis: Critical Impact of Phagosomal Acidification Control and Demonstration of Occurrence In Vivo. *PLoS Pathog.* **2015**, *11* (2), e1004650.

(64) Jamwal, S. V.; Mehrotra, P.; Singh, A.; Siddiqui, Z.; Basu, A.; Rao, K. V. S. Mycobacterial Escape from Macrophage Phagosomes to the Cytoplasm Represents an Alternate Adaptation Mechanism. *Sci. Rep.* **2016**, *6* (February), 23089.

(65) Chandra, P.; Ghanwat, S.; Matta, S. K.; Yadav, S. S.; Mehta, M.; Siddiqui, Z.; Singh, A.; Kumar, D. Mycobacterium Tuberculosis Inhibits RAB7 Recruitment to Selectively Modulate Autophagy Flux in Macrophages. *Sci. Rep.* **2015**, *5* (October), 16320.

(66) Abdallah, A. M.; Bestebroer, J.; Savage, N. D. L.; de Punder, K.; van Zon, M.; Wilson, L.; Korbee, C. J.; van der Sar, A. M.; Ottenhoff, T. H. M.; van der Wel, N. N.; Bitter, W.; Peters, P. J. Mycobacterial Secretion Systems ESX-1 and ESX-5 Play Distinct Roles in Host Cell Death and Inflammasome Activation. *J. Immunol.* **2011**, *187* (9), 4744–4753.

(67) Martin, C. J.; Booty, M. G.; Rosebrock, T. R.; Nunes-Alves, C.; Desjardins, D. M.; Keren, I.; Fortune, S. M.; Remold, H. G.; Behar, S. M. Efferocytosis Is an Innate Antibacterial Mechanism. *Cell Host Microbe* **2012**, *12* (3), 289–300.

(68) Liu, Y.; Zhang, Q.; Hu, M.; Yu, K.; Fu, J.; Zhou, F.; Liu, X. Proteomic Analyses of Intracellular Salmonella Enterica Serovar Typhimurium Reveal Extensive Bacterial Adaptations to Infected Host Epithelial Cells. *Infect. Immun.* **2015**, *83* (7), 2897–2906.

(69) Patiño, S.; Alamo, L.; Cimino, M.; Casart, Y.; Bartoli, F.; García, M. J.; Salazar, L. Autofluorescence of Mycobacteria as a Tool for Detection of Mycobacterium Tuberculosis. *J. Clin. Microbiol.* **2008**, *46* (10), 3296–3302.

(70) Wong, C.; Ha, N. P.; Pawlowski, M. E.; Graviss, E. A.; Tkaczyk, T. S. Differentiating between Live and Dead Mycobacterium Smegmatis Using Autofluorescence. *Tuberculosis* **2016**, *101*, S119–S123.

(71) Shetty, A.; Dick, T. Mycobacterial Cell Wall Synthesis Inhibitors Cause Lethal ATP Burst. *Front. Microbiol.* **2018**, *9* (AUG), 1–9.